Measurement of the ^{242m}Am neutron-induced reaction cross sections

M. Q. Buckner, C. Y. Wu, R. A. Henderson, B. Bucher, N. Wimer, A. Chyzh, T. A. Bredeweg, B. Baramsai, A. Couture, M. Jandel, S. Mosby, and J. L. Ullmann (DANCE Collaboration)

Phys. Rev. C **95**, 024610 — Published 17 February 2017

DOI: 10.1103/PhysRevC.95.024610

Measurement of the ^{242m}Am neutron-induced reaction cross sections

M. Q. Buckner,[1,*] C. Y. Wu,[1] R. A. Henderson,[1] B. Bucher,[1] N. Wimer,[1] A. Chyzh,[2] T. A. Bredeweg,[3] B. Baramsai,[3] A. Couture,[3] M. Jandel,[3] S. Mosby,[3] and J. L. Ullmann[3]

[1] *Lawrence Livermore National Laboratory, Livermore, CA 94550*
[2] *North Carolina State University, Raleigh, NC 27695*
[3] *Los Alamos National Laboratory, Los Alamos, NM 87544*

(Dated: January 10, 2017)

The neutron-induced reaction cross sections of ^{242m}Am were measured at the Los Alamos Neutron Science Center using the Detector for Advanced Neutron-Capture Experiments array along with a compact parallel-plate avalanche counter for fission-fragment detection. A new neutron-capture cross section was determined, and the absolute scale was set according to a concurrent measurement of the well-known ^{242m}Am(n,f) cross section. The (n,γ) cross section was measured from thermal to an incident energy of 1 eV at which point the data quality was limited by the reaction yield in the laboratory. Our new ^{242m}Am fission cross section was normalized to ENDF/B-VII.1 to set the absolute scale, and it agreed well with the (n,f) cross section reported by Browne *et al.* from thermal energy to 1 keV. The average absolute capture-to-fission ratio was determined from thermal to E_n = 0.1 eV, and it was found to be 26(4)% as opposed to the ratio of 19% from the ENDF/B-VII.1 evaluation.

I. INTRODUCTION

The actinide ^{242m}Am has unique attributes that make it suitable for numerous energy-related applications. Produced by ^{241}Am neutron capture, ^{242m}Am is a metastable isomer of americium-242 and features the highest measured thermal-fission cross section of any known nucleus [1, 2]—nearly an order of magnitude greater than the ^{235}U and ^{239}Pu thermal-fission cross sections. The high amplitude of the ^{242m}Am thermal-fission cross section is attributed to a low-energy ^{242m}Am(n,f) resonance, at $E_{n,R} = 0.178$ eV [3], with a large neutron width [4]. With a half-life of $t_{1/2}$ = 141(2) years [5], the properties of ^{242m}Am make it an appealing nuclear fuel. Applications, including a space reactor [6–15], a nuclear engine [16], a small-core reactor [17, 18], and a fission battery [19–25], have been proposed.

The ^{242m}Am fission channel has been well studied by accelerator-based [4, 26–28] and detonation-based [29, 30] experiments despite some discrepancies among the results [31]. For instance, the measured thermal-fission cross sections differ by $\approx$ 10% with quoted uncertainties of $\approx$ 3–5% for the experiments performed by Dabbs *et al.* [27] and Browne *et al.* [4]. These two measurements were the first experiments performed with high-purity ^{242m}Am samples (>99%). Table I (top) lists these ^{242m}Am thermal-fission cross sections along with others from the literature. In the ENDF/B-VII.1 evaluation [32], the ^{242m}Am(n,f) cross section relies on analysis performed by Ref. [33]. Due to their relatively high precision, data from Browne *et al.* [4] and Fursov *et al.* [28] dominate the evaluated cross section [32, 33]. The electromagnetic properties of low-lying states in ^{242}Am were studied recently by Coulomb excitation in Ref. [34].

TABLE I. ^{242m}Am thermal-fission (top) and thermal-capture (bottom) cross sections reported in the literature.

Reference	σ_{th}(n,f) (b)
Hulet *et al.* [1][1]	6390±500
Wolfsberg *et al.* [2][2]	7200±300
Bowman *et al.* [26][3]	6600±300
Wolfsberg and Ford [35][4]	7600±300
Zhuravlev *et al.* [36]	6080±500
Dabbs *et al.* [27]	6950±250
Browne *et al.* [4]	6328±320
Kai *et al.* [37]	5850±250
Bringer *et al.* [38][5]	6855.97±657
Reference	**σ_{th}(n,γ) (b)**
Street Jr. *et al.* [39]	2000±300
Bringer *et al.* [38][5]	1161±111

[1] Corrected to 6010±500 by Ref. [26].
[2] Corrected to 6830±300 by Ref. [26].
[3] Weighted mean of reanalyzed cross sections from Refs. [1, 2].
[4] Reanalysis of Ref. [2].
[5] The Mini-INCA project.

The neutron-capture cross section is not well measured, and only a few values at thermal neutron energy—25.3 meV—have been reported (see Tab. I). These measurements differ by nearly a factor of two with quoted uncertainties of about 10 to 15%. The ^{242m}Am(n,γ) cross section is valuable for the calculation of heavy actinide concentrations in nuclear fuel [40], actinide waste recycling, and heavy isotope production [4, 41]. Also, as pointed out by Rubbia [13], the ^{242m}Am neutron-capture cross section is important for ^{242m}Am-based propulsion and energy systems.

In this work, the ^{242m}Am(n,f) and ^{242m}Am(n,γ) cross sections were measured concurrently at the Los Alamos Neutron Science Center (LANSCE) using the Detector

* Corresponding author: buckner4@llnl.gov

for Advanced Neutron-Capture Experiments (DANCE) array [42] in combination with a parallel-plate avalanche counter (PPAC) [43]. The fission cross section was measured from thermal to an incident neutron energy (E_n) of 1 keV, and the capture cross section was measured from thermal to E_n = 1 eV. Our ^{242m}Am(n,f) cross section was normalized to the ENDF/B-VII.1 [32] fission cross section, and the ^{242m}Am(n,γ) cross section is reported with respect to our fission cross section. Details of the experiment, the analysis, and results are described in the sections below.

II. EXPERIMENT

Cross sections of neutron-induced reactions on ^{242m}Am were measured at the LANSCE Lujan Neutron Scattering Center [44] with DANCE. The DANCE array consists of 160 equal-volume, equal-solid-angle BaF_2 crystals arranged in a 4π geometry. DANCE has been used to measure neutron-induced reactions on actinides including ^{237}Np [45], ^{241}Am [46], ^{235}U [47], ^{238}Pu [48], ^{239}Pu [49], ^{238}U [50], and ^{242}Pu [51]. The detector array is located at the end of a flight path 20.25 m from the neutron source. Spallation neutrons are produced at the source by bombarding a tungsten target with 800-MeV protons at a 20 Hz repetition rate; the neutrons are then thermalized with a water moderator [52]. The incident neutron energy spectrum produced, determined by the time-of-flight difference between event detection and the beam pulse, spans an energy range from thermal to several hundred keV. The experiment was fielded over 11 days with a PPAC containing a ^{242m}Am target installed within DANCE. It is necessary that backgrounds induced by scattered neutrons be measured and subtracted from data collected in the inclusive data acquisition mode (referred to as the *inclusive mode* in this paper). The background measurement in the inclusive mode was fielded with one day of beam incident upon a blank target in a duplicate PPAC.

The electroplating cell described in Ref. [53] was used at Lawrence Livermore National Laboratory (LLNL) to fabricate a double-sided, electroplated ^{242m}Am target with a mass of ≈0.140 mg, an enrichment of 99.1%, and an ≈1.0 cm diameter active area. The ^{241}Am contamination in the sample was measured with the mass spectrometer at LLNL and was found to be 0.92(23)%. Curium-242 builds up as ^{242m}Am decays to ^{242g}Am—by isomeric transition—that subsequently β-decays [4]. It is necessary to remove ^{242}Cm from the sample before target fabrication because the α-decay rate ($t_{1/2}$ = 163 days) can overwhelm the PPAC. Because of this, it is important to minimize delays between target production and the experiment. Figure 1 shows a schematic of the production and destruction reaction chains for ^{242m}Am [33].

After preparation, our target was installed within the PPAC by sandwiching it between two 1.8 μm thick aluminum foils—the PPAC anode. Additional 1.8 μm thick aluminum foils—the PPAC cathodes—were mounted on either side of the target with 3 mm gaps between the anode and the cathodes. The PPAC's entrance and exit windows are 13 μm thick Kapton foils. A similar PPAC design was used in several previous experiments conducted with DANCE including a ^{252}Cf spontaneous fission measurement [54] and the recent ^{242}Pu neutron-capture cross section measurement [51]. The PPAC was operated with ≈4 Torr of isobutane stabilized by a gas-handling system, and it was biased up to ≈400 V. The typical pulse height for fission events is several hundred mV.

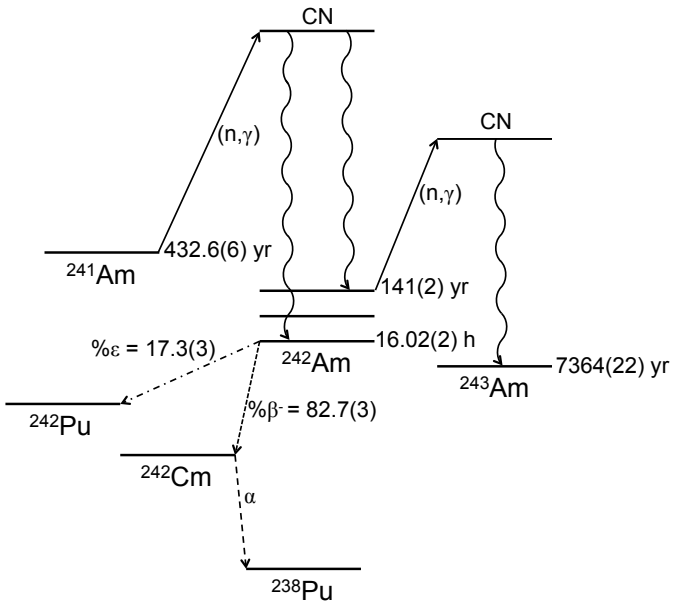

FIG. 1. The nuclear reaction chain for isotopes of americium [5, 33, 55, 56]. "CN" is an abbreviation of "compound nucleus."

III. ANALYSIS

In this work, the determination of the fission cross section is dependent upon the PPAC−DANCE coincidence condition and the associated γ-ray spectra. Meanwhile, deriving the neutron-capture cross section depends upon the total γ-ray energy (E_{sum}) spectrum and the cluster multiplicity (M_{cl}) measured with the DANCE array in the inclusive mode. The γ-ray cluster multiplicity requires that γ rays detected with adjacent BaF_2 crystals triggered are grouped together, within a given timing window, to minimize over-counting the γ-ray multiplicity due to Compton scattering. Appropriate gates were set on all of these quantities to optimize the true-to-background ratio and improve the precision of the measurement. As a result, detector efficiencies due to the gating are required to extract the cross section from the data. Efficiencies for both the PPAC (ϵ_{PPAC}) and

DANCE ($\epsilon_{\rm DANCE}$) are described in the subsections below.

During the first day of data acquisition (DAQ), data were collected with a 10 ms timing window in order to probe the incident neutron energy down to thermal energy. Over the remainder of the experiment, this timing window was narrowed to 2 ms (corresponding to $E_n \geq 0.5$ eV) in order to lower the data acquisition rate to a sustainable level. In this paper, analysis performed at thermal energy corresponds to spectra that cover incident neutron energies from thermal to several hundred keV collected during the first period of data acquisition (referred to as the *first period* in this work). Analysis corresponding to incident neutron energies above 0.5 eV includes data collected with both the 10 ms and 2 ms timing windows and is referred to as the *entire period* of data acquisition in this text.

A. PPAC efficiency

The ^{242m}Am(n,f) reaction was measured with parallel-plate avalanche counter events in coincidence with the detection of DANCE γ rays emitted by fission fragments. The relative fission cross section was determined and then normalized to the ENDF/B-VII.1 [32] fission cross section to obtain the absolute scale. In order to derive this cross section, the PPAC efficiency was established by comparing prompt fission γ-ray spectra collected either with or without a PPAC coincidence requirement. Gates on the PPAC pulse height and PPAC−DANCE coincident timing spectrum, shown in Fig. 2, allowed a sample of the γ rays associated with the fission fragments to be isolated from inclusive DANCE γ-ray spectra. An $\approx$ 1.5 ns timing resolution was observed in the PPAC−DANCE coincident timing spectrum, and a 6-ns coincidence gate was set around the timing peak. Figure 3 shows the γ-ray cluster multiplicity versus summed γ-ray energy spectrum produced by this gating condition. In DANCE, fission is characterized by high-multiplicity, high-γ-ray-energy events, and the dashed rectangle in the figure emphasizes the γ rays associated with the fission fragments in the inclusive spectrum—events with cluster multiplicity $M_{cl} \geq 8$. The same multiplicity constraint was placed on inclusive DANCE spectra, and the efficiency of the PPAC was determined from the ratio between inclusive mode events and events in coincidence with the PPAC (see Fig. 4). The weighted mean of PPAC efficiencies over several incident neutron energy bins was found to be 32.9(10)% for the first period. The PPAC efficiency dropped over the course of the experiment, and it was found to be 26.0(11)% for the entire period. The efficiency degradation can be prevented in future experiments by refreshing the isobutane gas in the counter regularly. The PPAC absolute efficiency was low in this experiment—almost a factor of two lower than previous measurements—because the threshold on the PPAC was set too high.

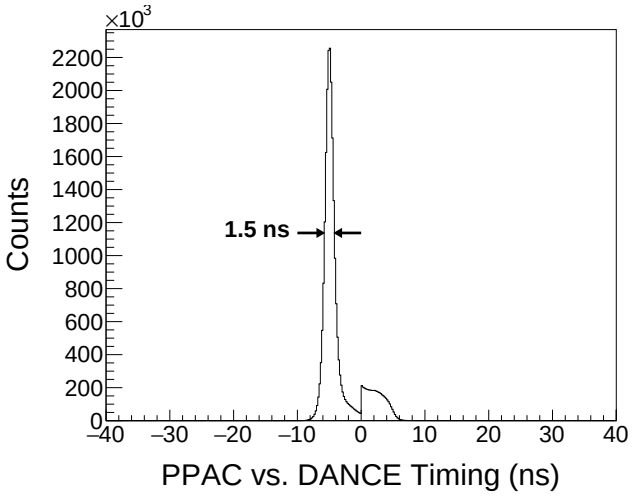

FIG. 2. The time difference between γ rays detected by the DANCE array and charged particles detected by the PPAC for the ^{242m}Am(n,f) reaction. The timing resolution is $\approx$1.5 ns for the peak at $\approx$-5 ns. A 6-ns gate was placed around this peak. The discontinuity at 0 ns is an artifact of the timing algorithm.

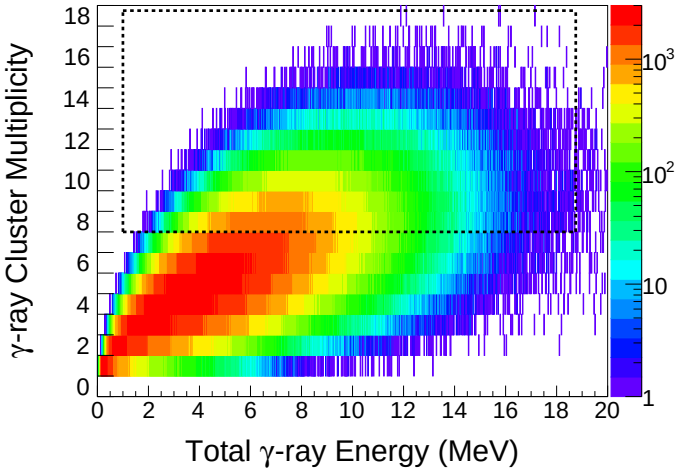

FIG. 3. The measured cluster multiplicity versus total γ-ray energy for the gated PPAC. The dashed box indicates the high-multiplicity ($M_{cl} \geq 8$) region of the spectrum attributed to neutron-induced fission of ^{242m}Am in the inclusive mode.

B. DANCE efficiency

The DANCE efficiency depends on the gates placed on the cluster multiplicity and the summed γ-ray energy in the inclusive mode, and it is the product of their respective gating efficiencies. During the first stage of data analysis, γ-ray energies deposited in DANCE were summed over a 200-ns coincident timing window, and then "time alignment" was applied to the 160 BaF_2 scin-

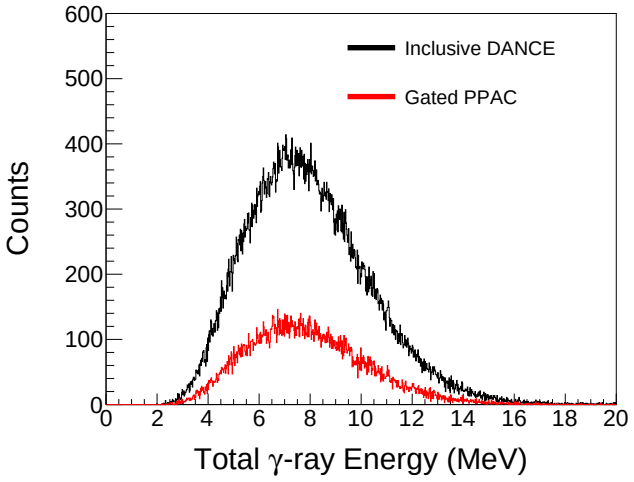

FIG. 4. The E_{sum} spectrum collected in the inclusive mode (black) with the multiplicity condition $M_{cl} \geq 8$ is compared to the PPAC E_{sum} (red) with the PPAC−DANCE coincident timing constraint and the same multiplicity threshold. These spectra were derived from the first period data with incident neutron energy bin $E_n = 0.5-1$ eV.

tillation crystals. A reference crystal was selected for the alignment, and the timing for each subsequent crystal was corrected for each run, based on the time difference relative to the reference crystal [46, 51]. After alignment, γ-ray energies were summed over a narrow, 6-ns coincident time window. The analysis that follows was also performed with the coincident time window set to 10 ns to estimate systematic uncertainties. Standard γ-ray calibration sources (^{22}Na and ^{60}Co) and the ^{226}Ra α-decay inherent to the BaF_2 crystals were used to energy-align the DANCE γ-ray spectra. During the experiment, the ^{6}Li(n,α) reaction rate was measured downstream from the DANCE array to monitor the neutron flux.

The inclusive E_{sum} spectrum must undergo several background subtractions to isolate the ^{242m}Am(n,γ) reaction channel. Figure 5 outlines the procedure for extracting the ^{242m}Am(n,γ) signal from the inclusive data; the incident neutron energy bin $E_n = 0.1-0.5$ eV with cluster multiplicity $M_{cl} = 4$ is shown as an example. The first step involved scaling the fission E_{sum} spectrum by the PPAC efficiency and subtracting it from the inclusive E_{sum} spectrum for each cluster multiplicity (see Fig. 5a). Next, a scaled presampled E_{sum} spectrum was subtracted (see Fig. 5b). Presampled spectra correspond to data collected before the proton-beam time-reference signal and rely upon the look-back window of the DAQ digitizers—see Ref. [49] for more information. These spectra arise from long-lived fission fragments that build up in the sample. The presampled E_{sum} spectra were scaled by the ratio of the time width of the neutron energy bin and the look-back window [49] for each cluster multiplicity and each neutron energy bin. Finally, the scaled environmental background was subtracted (see Fig. 5c). Environmental background spectra were collected with neutron beam incident upon a duplicate PPAC setup that contained a blank target. These spectra were normalized to the inclusive E_{sum} spectra that remained after the first two subtractions. The area

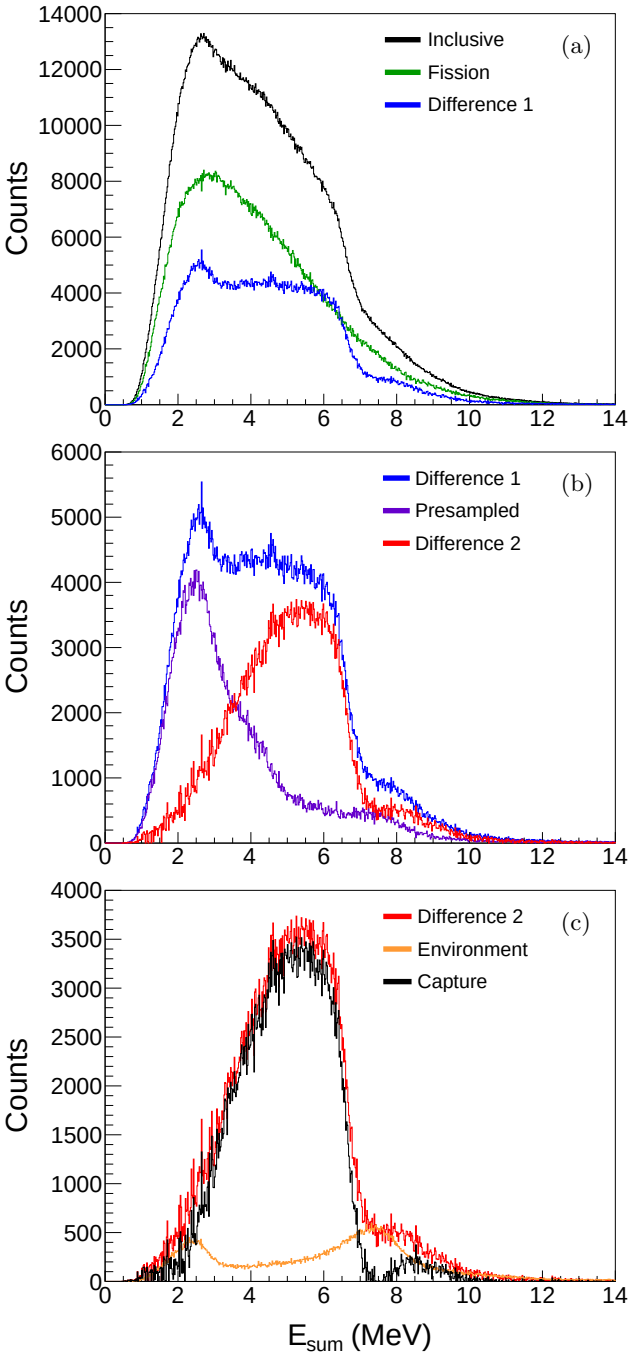

FIG. 5. Background subtractions of the scaled (a) fission, (b) presampled, and (c) environmental components were subtracted from inclusive E_{sum} spectra to isolate the (n,γ) channel, shown in (c). Only E_{sum} spectra for cluster multiplicity $M_{cl} = 4$ and incident neutron energy bin $E_n = 0.1-0.5$ eV are shown. The ^{242m}Am(n,γ) Q value is 6365 keV [3, 57].

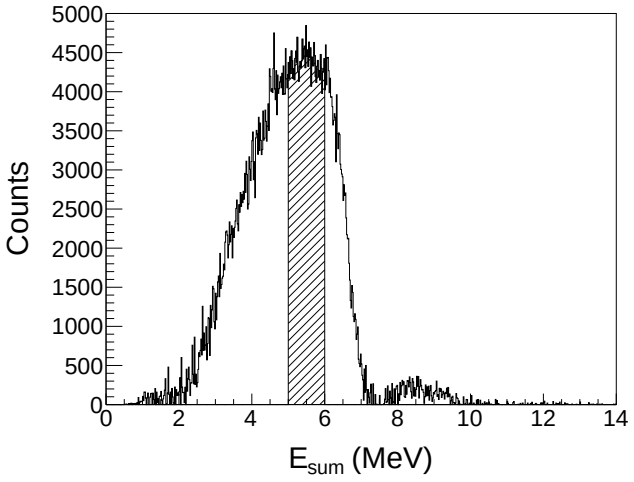

FIG. 6. The background-subtracted E_{sum} spectrum for ^{242m}Am(n,γ) at E_n = 0.1−0.5 eV. Only cluster multiplicities 4 and 5 are shown, and the E_{sum} = 5.0−6.0 MeV region, representing the peak area, is shaded.

selected for this normalization, E_{sum} = 7−8 MeV, corresponds to γ rays produced by barium isotopes, in the BaF_2 crystals, capturing scattered neutrons [58].

In Fig. 5c, the background-subtracted E_{sum} spectrum (black) exhibits the typical characteristics of the (n,γ) channel—see Fig. 4a in Ref. [51] as an example. Background subtraction was effective for cluster multiplicities M_{cl} = (4,5), and Fig. 6 shows the (n,γ) E_{sum} for incident neutron energy bin E_n = 0.1−0.5 eV. The E_{sum} efficiency is the ratio between the peak area (5.0−6.0 MeV in this case) and the total area. The weighted mean of E_{sum} efficiencies over many incident neutron energy bins was found to be 33.0(8)% for cluster multiplicities M_{cl} = (4,5). The derived E_{sum} efficiency for events with M_{cl} = (3,4) was 29% and is considered less reliable because backgrounds dominated the M_{cl} = 3 events.

The quality of the data deteriorated for the ^{242m}Am(n,γ) channel at higher incident neutron energies, and it became difficult to isolate the (n,γ) signal after subtracting the backgrounds. Figure 7 shows the E_n = 10−100 eV bin with cluster multiplicity M_{cl} = 4. The inclusive spectrum (red) and the scaled backgrounds—fission (blue), presampled (green), and environmental (purple)—are shown. The final (n,γ) signal (orange) is weak, and the E_{sum} efficiency cannot be extracted reliably. In general, conclusions about the neutron-capture cross section cannot be drawn above E_n = 1 eV.

Following the steps described in the sections above, the (n,γ) E_{sum} spectrum was produced for each cluster multiplicity from 2 to 9. These background subtracted E_{sum} spectra were integrated from E_{sum} = 2.25−7.25 MeV, and the integrands were then used to calculate the cluster multiplicity efficiencies for each incident neutron energy bin. Cluster multiplicities 0 and 1 could not be derived from the data and were estimated using a Poisson distribution (an analytical approximation of the measured shape) that was fit to M_{cl} = 2−9. The events with cluster multiplicities 0 and 1 were estimated to be ≈4% of the total. Figure 8 shows the cluster multiplicity distribution for the incident neutron energy bin E_n = 0.05−0.1 eV. The Poisson distribution is shown as a solid line and was fit to M_{cl} = 2−9. Multiplicity efficiencies were calculated for different incident neutron energy bins below 1 eV, and the weighted mean was adopted as the detec-

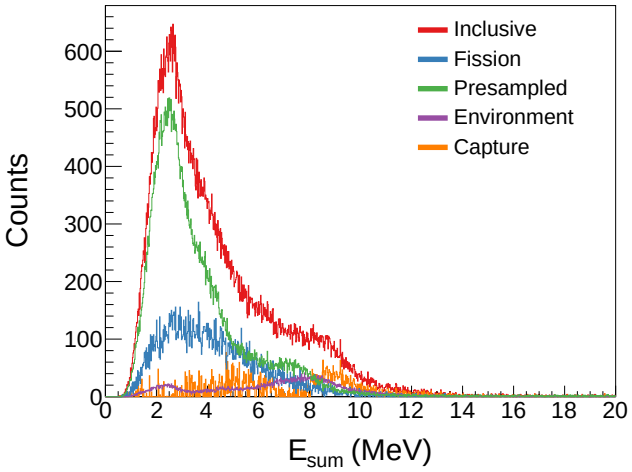

FIG. 7. The E_{sum} spectrum for the ^{242m}Am(n,γ) reaction channel, shown in orange, after the subtraction of scaled fission (blue), presampled (green), and environmental (purple) backgrounds from the inclusive (red) spectrum. Only the incident neutron energy bin E_n = 10−100 eV with cluster multiplicity 4 is shown. The ^{242m}Am(n,γ) signal deteriorates above E_n = 1 eV.

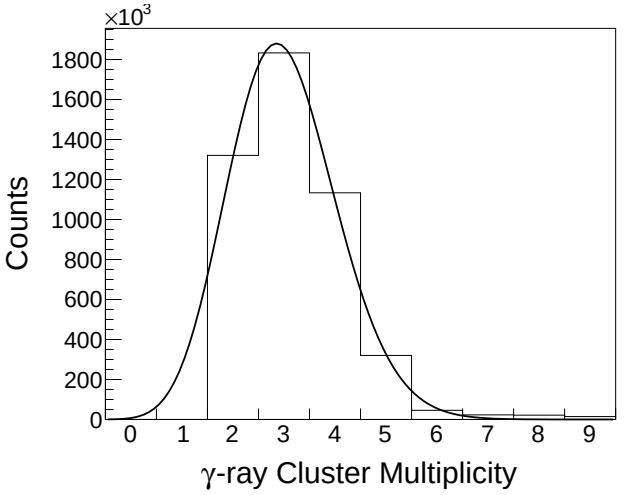

FIG. 8. The cluster multiplicity spectrum for the ^{242m}Am(n,γ) reaction and energy bin E_n = 0.05−0.1 eV. The solid line is a Poisson distribution fit to M_{cl} = 2−9 to estimate multiplicities 0 and 1.

tor multiplicity efficiency. For cluster multiplicities M_{cl} = (4,5), the efficiency was 30(2)%, and for cluster multiplicities M_{cl} = (3,4), it was 61%. The DANCE array efficiency is the product of the M_{cl} and E_{sum} efficiencies; for M_{cl} = (4,5), ϵ_{DANCE} = 10.0(7)%, and for M_{cl} = (3,4), ϵ_{DANCE} = 18%. The ϵ_{DANCE} value of 10.0(7)% with M_{cl} = (4,5) is considered to be the more reliable value and was used to derive the ^{242m}Am(n,γ) cross section.

IV. RESULTS

To improve the precision of extracted neutron-induced reaction cross sections on ^{242m}Am, it was necessary to gate on observables, such as the E_{sum}, M_{cl}, and the coincident time window between DANCE and PPAC. The impact on the efficiency of both detector systems due to this gating requirement was addressed in the sections above. From the derived ϵ_{PPAC} and ϵ_{DANCE}, both the neutron-induced fission and neutron-capture cross sections can be determined and are presented in the subsections below.

A. Absolute capture-to-fission cross section ratio

For neutron-induced reactions on ^{242m}Am, the absolute ratio of capture-to-fission cross sections can be determined directly from the data since both reactions were measured concurrently in this experiment. After corrections for the detector efficiencies, the relative ^{242m}Am(n,f) cross section was determined for E_n from thermal to about 1 keV, and the relative ^{242m}Am(n,γ) cross section was established for E_n from thermal to about 1 eV. The (n,f) cross section for E_n from thermal to 0.5 eV was derived from events collected in the first period, and above 0.5 eV, the cross section was determined from events collected during the entire period. The (n,γ) cross section was derived solely from the first period data. The average absolute ratio of capture-to-fission cross sections was measured to be 26(4)% for E_n from thermal to about 0.1 eV. This value was determined from the events with M_{cl} = (4,5) and is consistent with the value of 25% from the events with M_{cl} = (3,4). For comparison, the values reported by ENDF/B-VII.1 [32] and Ref. [38] were 19% and 16.9(23)%, respectively, at thermal energy.

B. (n,γ) and (n,f) cross sections

The absolute ^{242m}Am(n,f) cross section scale was obtained by normalizing the relative fission cross section to the evaluated cross section [32] for E_n from thermal to about 100 eV. Our absolute fission cross section is shown in Fig. 9 along with the Browne *et al.* [4] cross section. Note that the 5% systematic uncertainty from Ref. [4] is included in the figure. The two measurements agree well,

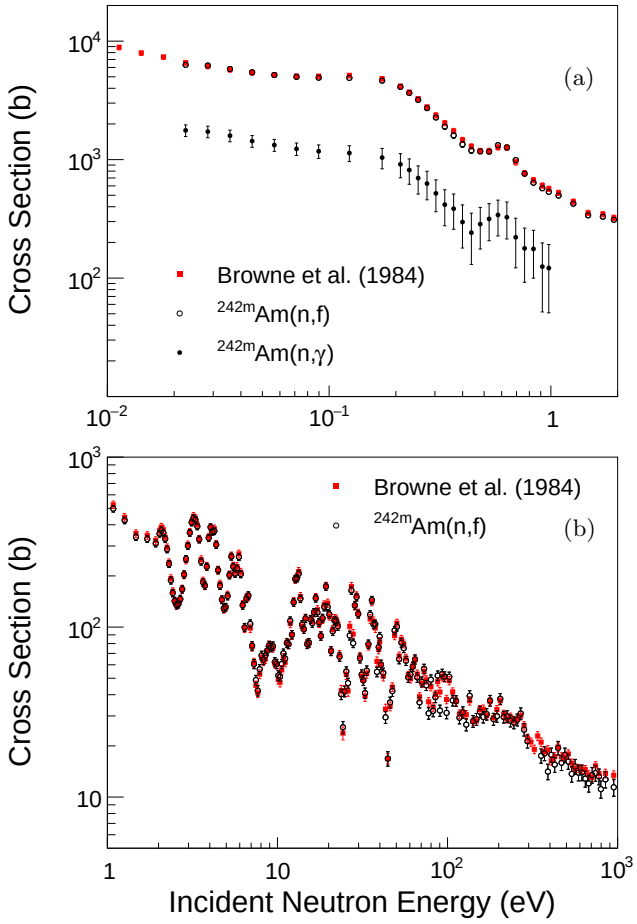

FIG. 9. The ^{242m}Am(n,f) cross section (open black circles) is plotted alongside the Browne *et al.* [4] (red squares) data for incident neutron energy ranges of (a) thermal to 2.0 eV and (b) 1.0 eV to 1.0 keV. The absolute neutron-capture cross section (filled black circles) is plotted for E_n from thermal to 1 eV.

but above $E_n \approx 300$ eV, our data are $\approx 8\%$ lower; however, the measurements still agree within one standard deviation. Our thermal fission cross section, σ_{th}(n,f) = 6200 $\pm$ 200 b, is the same as the evaluated value reported by Mughabghab [3]. The absolute neutron-capture cross section was obtained with respect to our absolute fission cross section and is shown in Fig. 9a from thermal to 1 eV. The cross section at thermal energy, $\sigma_{th}(n,\gamma) = 1720 \pm 190$ b, is higher than the value of 1161 $\pm$ 111 b reported by the Mini-INCA project [38] but agrees with the Mughabghab [3] evaluation and the Street Jr. *et al.* [39] measurement within uncertainty. The new ^{242m}Am(n,γ) cross sections in Fig. 9 are tabulated in Tab. II.

TABLE II. ^{242m}Am neutron-capture cross sections. The uncertainty on the neutron energy represents the bin width.

Neutron energy (eV)	Cross section (b)
0.023(3)	1800(200)
0.028(3)	1720(190)
0.036(4)	1590(180)
0.045(5)	1430(160)
0.057(6)	1330(150)
0.071(8)	1230(150)
0.090(10)	1180(150)
0.12(2)	1140(170)
0.17(3)	1000(200)
0.210(10)	900(200)
0.230(10)	800(200)
0.252(11)	700(190)
0.276(13)	630(170)
0.303(14)	520(160)
0.332(15)	420(140)
0.364(17)	390(130)
0.399(18)	300(120)
0.44(2)	240(110)
0.48(2)	290(110)
0.53(2)	320(110)
0.58(3)	340(110)
0.63(3)	330(110)
0.69(3)	220(100)
0.76(4)	180(90)
0.83(4)	180(80)
0.92(4)	130(70)
0.98(2)	120(70)

V. SUMMARY

The neutron-induced reactions on ^{242m}Am have been studied using the DANCE array together with a compact PPAC for fission-fragment detection at the LANSCE Lujan Neutron Scattering Center. The ^{242m}Am(n,f) cross section was derived for E_n from thermal to about 1 keV and agrees with the Browne *et al.* [4] results. The absolute ^{242m}Am(n,γ) cross section was obtained, for E_n from thermal to about 1 eV, with respect to our measured fission cross section. Our results represent the first direct measurement of the ^{242m}Am(n,γ) reaction above thermal energy. At thermal energy, the (n,γ) cross section is about 30% higher than the most recently measured value from the Mini-INCA project [38], but it agrees with the evaluated value [3] and one other measurement [39] within uncertainty. Despite the limited range of the incident neutron energy for the measured (n,γ) cross section, the definite (n,γ)/(n,f) cross section ratio will have important consequences on the simulations of many ^{242m}Am-based applications, such as propulsion and energy systems. However, extending the measurement into the resonance region would further improve model calculations and simulations of applications. As a result, the neutron-induced reactions on ^{242m}Am warrant further study.

ACKNOWLEDGMENTS

This measurement was performed under the auspices of the US Department of Energy by Lawrence Livermore National Security, LLC under contract DE-AC52-07NA27344 and by Los Alamos National Security, LLC under contract DE-AC52-06NA25396. Additional funding was provided by the U.S. DOE/NNSA Office of Defense Nuclear Nonproliferation Research and Development.

[1] E. K. Hulet, R. W. Hoff, H. R. Bowman, and M. C. Michel, Physical Review **107**, 1294 (1957).
[2] K. Wolfsberg, G. P. Ford, and H. L. Smith, Journal of Nuclear Energy. Parts A/B. Reactor Science and Technology **20**, 588 (1966).
[3] S. F. Mughabghab, *Atlas of Neutron Resonances: Resonance Parameters and Thermal Cross Sections. Z= 1−100* (Elsevier, 2006).
[4] J. C. Browne, R. M. White, R. E. Howe, J. H. Landrum, R. J. Dougan, and R. J. Dupzyk, Phys. Rev. C **29**, 2188 (1984).
[5] Y. A. Akovali, Nuclear Data Sheets **96**, 177 (2002).
[6] Y. Ronen and M. J. Leibson, Trans. Israel Nucl. Soc. **14**, 42 (1987).
[7] Y. Ronen and M. J. Leibson, Nuclear Science and Engineering **99**, 278 (1988).
[8] G. Chapline, Nucl. Instrum. Methods A **271**, 207 (1988).
[9] H. Ludewig, O. Lazareth, S. Mughabghab, K. Perkins, and J. R. Powell, *Small propulsion reactor design based on particle bed reactor concept*, Tech. Rep. (Brookhaven National Lab., Upton, NY (USA), 1989).
[10] T. Kammash, D. L. Galbraith, and T.-R. Jan, in *Proceedings of the 10th Symposium on Space Nuclear Power and Propulsion, Albuquerque, NM, USA*, Vol. 271 (The American Institute of Physics, 1993).
[11] C. Rubbia, in *Proceedings of The Ninth International Conference on Emerging Nuclear Energy Systems, Keynote, Tel-Aviv, Israel* (1998) p. 4.
[12] Y. Ronen and E. Shwageraus, Nucl. Instrum. Methods A **455**, 442 (2000).
[13] C. Rubbia, "Method and device for heating gas from a thin layer of nuclear fuel, and space engine using such method," U.S. Patent 0,080,907, Mar. 28, 2002.
[14] Y. Ronen and G. Raitses, Nucl. Instrum. Methods A **522**, 558 (2004).
[15] M. Augelli, G. F. Bignami, and G. Genta, Acta Astronautica **82**, 153 (2013).
[16] Y. Ronen, M. Aboudy, and D. Regev, Ann. Nucl. Energy **27**, 85 (2000).

[17] Y. Ronen, M. Aboudy, and D. Regev, Nucl. Technol. **129**, 407 (2000).

[18] Y. Ronen, M. Aboudy, and D. Regev, Nuclear science and engineering **138**, 295 (2001).

[19] S. L. Soo, *Direct energy conversion* (Prentice-Hall, Engelwood Cliffs, NJ, 1968).

[20] G. H. Miley, *Direct conversion of nuclear radiation energy*, Tech. Rep. (University of Illinois, Urbana-Champaign, IL, 1970).

[21] G. Chapline and Y. Matsuda, Fusion Technol. **20**, 719 (1991).

[22] S. A. Slutz, D. B. Seidel, R. J. Lipinski, G. E. Rochau, and L. C. Brown, Physics of Plasmas **10**, 2983 (2003).

[23] P. V. Tsvetkov, R. R. Hart, and T. A. Parish, in *Proceedings of the 11th International Conference on Nuclear Engineering (ICONE 11)* (2003) pp. 20–23.

[24] Y. Ronen, A. Hatav, and N. Hazenshprung, Nucl. Instrum. Methods A **531**, 639 (2004).

[25] Y. Ronen, M. Kurtzhand, L. Droizman, and E. Shwageraus, Journal of propulsion and power **23**, 874 (2007).

[26] C. D. Bowman, G. F. Auchampaugh, S. C. Fultz, and R. W. Hoff, Physical Review **166**, 1219 (1968).

[27] J. W. T. Dabbs, C. E. Bemis Jr, S. Raman, R. J. Dougan, and R. W. Hoff, Nuclear Science and Engineering **84**, 1 (1983).

[28] B. I. Fursov, B. F. Samylin, G. N. Smirenkin, and V. N. Polynov, in *Proc. Int. Conf. Nucl. Data for Science and Technol., Gatlinburg, Tenn*, Vol. 1 (1994) p. 269.

[29] P. A. Seeger, A. Hemmendinger, and B. C. Diven, Nucl. Phys. A **96**, 605 (1967).

[30] E. V. Fomushkin, G. F. Novoselov, Y. I. Vinogradov, V. V. Gavrilov, V. I. Inkov, B. K. Maslennikov, V. N. Polynov, V. M. Surin, and A. M. Shvetsov, Yadernaya Fizika **33**, 620 (1981).

[31] V. M. Maslov, E. S. Sukhovitskij, Y. V. Porodzinskij, and G. B. Morogovskij, Rep. INDC (BLR)-007 (1997).

[32] M. B. Chadwick, M. Herman, P. Obložinskỳ, M. E. Dunn, Y. Danon, A. C. Kahler, D. L. Smith, B. Pritychenko, G. Arbanas, R. Arcilla, *et al.*, Nuclear Data Sheets **112**, 2887 (2011).

[33] P. Talou, T. Kawano, P. G. Young, M. B. Chadwick, and R. E. MacFarlane, Nuclear science and engineering **155**, 84 (2007).

[34] A. B. Hayes, D. Cline, K. J. Moody, I. Ragnarsson, C. Y. Wu, J. A. Becker, M. P. Carpenter, J. J. Carroll, D. Gohlke, J. P. Greene, *et al.*, Physical Review C **82**, 044319 (2010).

[35] K. Wolfsberg and G. P. Ford, Phys. Rev. C **3**, 1333 (1971).

[36] K. D. Zhuravlev, N. I. Kroshkin, and A. P. Chetverikov, Atomic Energy **39**, 285 (1975).

[37] T. Kai, K. Kobayashi, S. Yamamoto, H.-J. Cho, Y. Fujita, I. Kimura, Y. Ohkawachi, and T. Wakabayashi, Annals of Nuclear Energy **28**, 723 (2001).

[38] O. Bringer, I. AlMahamid, S. Chabod, F. Chartier, E. Dupont, A. Letourneau, P. Mutti, L. Oriol, S. Panebianco, and C. Veyssière, in *International Conference on Nuclear Data for Science and Technology* (EDP Sciences, 2007) pp. 619–622.

[39] K. Street Jr., A. Ghiorso, and S. G. Thompson, Physical Review **85**, 135 (1952).

[40] J. L. Crandall, in *Proc. Int. Conf. on Constructive Uses of Atomic Energy, Washington, D.C.* (1968) p. 193.

[41] S. Raman, in *IAEA advisory group meeting on transactinium isotope nuclear data, Karlsruhe, F.R. Germany* (1975) p. 39.

[42] M. Heil, R. Reifarth, M. M. Fowler, R. C. Haight, F. Käppeler, R. S. Rundberg, E. H. Seabury, J. L. Ullmann, J. B. Wilhelmy, and K. Wisshak, Nucl. Instrum. Methods A **459**, 229 (2001).

[43] C. Y. Wu, A. Chyzh, E. Kwan, R. A. Henderson, J. M. Gostic, D. Carter, T. A. Bredeweg, A. Couture, M. Jandel, and J. L. Ullmann, Nucl. Instrum. Methods A **694**, 78 (2012).

[44] P. W. Lisowski, C. D. Bowman, G. J. Russell, and S. A. Wender, Nuclear Science and Engineering **106**, 208 (1990).

[45] E.-I. Esch, R. Reifarth, E. M. Bond, T. A. Bredeweg, A. Couture, S. E. Glover, U. Greife, R. C. Haight, A. M. Hatarik, R. Hatarik, *et al.*, Phys. Rev. C **77**, 034309 (2008).

[46] M. Jandel, T. A. Bredeweg, E. M. Bond, M. B. Chadwick, R. R. Clement, A. Couture, J. M. O'Donnell, R. C. Haight, T. Kawano, R. Reifarth, *et al.*, Phys. Rev. C **78**, 034609 (2008).

[47] M. Jandel, T. A. Bredeweg, E. M. Bond, M. B. Chadwick, A. Couture, J. M. O'Donnell, M. Fowler, R. C. Haight, T. Kawano, R. Reifarth, *et al.*, Phys. Rev. Lett. **109**, 202506 (2012).

[48] A. Chyzh, C. Y. Wu, E. Kwan, R. A. Henderson, J. M. Gostic, T. A. Bredeweg, A. Couture, R. C. Haight, H. Y. Lee, J. M. O'Donnell, *et al.*, Phys. Rev. C **88**, 044607 (2013).

[49] S. Mosby, T. A. Bredeweg, A. Chyzh, A. Couture, R. Henderson, M. Jandel, E. Kwan, J. M. O'Donnell, J. Ullmann, and C.-Y. Wu, Phys. Rev. C **89**, 034610 (2014).

[50] J. L. Ullmann, T. Kawano, T. A. Bredeweg, A. Couture, R. C. Haight, M. Jandel, J. M. O'Donnell, R. S. Rundberg, D. J. Vieira, J. B. Wilhelmy, *et al.*, Phys. Rev. C **89**, 034603 (2014).

[51] M. Q. Buckner, C.-Y. Wu, R. A. Henderson, B. Bucher, A. Chyzh, T. A. Bredeweg, B. Baramsai, A. Couture, M. Jandel, S. Mosby, *et al.*, Phys. Rev. C **93**, 044613 (2016).

[52] M. Mocko and G. Muhrer, Nucl. Instrum. Methods A **704**, 27 (2013).

[53] R. A. Henderson, J. M. Gostic, J. T. Burke, S. E. Fisher, and C. Y. Wu, Nucl. Instrum. Methods A **655**, 66 (2011).

[54] A. Chyzh, C. Y. Wu, E. Kwan, R. A. Henderson, J. M. Gostic, T. A. Bredeweg, R. C. Haight, A. C. Hayes-Sterbenz, M. Jandel, J. M. O'Donnell, *et al.*, Phys. Rev. C **85**, 021601 (2012).

[55] C. D. Nesaraja and E. A. McCutchan, Nuclear Data Sheets **121**, 695 (2014).

[56] C. D. Nesaraja, Nuclear Data Sheets **130**, 183 (2015).

[57] M. Wang, G. Audi, A. H. Wapstra, F. G. Kondev, M. MacCormick, X. Xu, and B. Pfeiffer, Chinese Physics C **36**, 1603 (2012).

[58] B. Baramsai, G. E. Mitchell, U. Agvaanluvsan, F. Bečvář, T. A. Bredeweg, A. Chyzh, A. Couture, D. Dashdorj, R. C. Haight, M. Jandel, *et al.*, Phys. Rev. C **85**, 024622 (2012).